Quantifying the Role of 3D Fault Geometry Complexities on Slow and Fast Earthquakes

J. Cheng[1,*,¶], H. S. Bhat[1], M. Almakari[1], B. Lecampion[2], P. Dubernet[1]

1. Laboratoire de Géologie, Ecole Normale Superieure, CNRS-UMR 8538, PSL Research University, Paris, France
2. Geo-Energy Lab - Gaznat Chair on Geo-Energy, Swiss Federal Institute of Technology in Lausanne, EPFL-ENAC-IIC-GEL, Station 18, Lausanne CH-1015, Switzerland

∗ Currently at Division of Geological and Planetary Sciences, California Institute of Technology.

¶ Corresponding author: jcheng95@caltech.edu

Key Points

- 3D simulations of two parallel faults show that interacting faults can generate slow slip events (SSEs), earthquakes, or complex sequences, while a single planar fault produces only earthquakes.
- We quantify fault interaction strength to understand how geometrical parameters control the occurrence and proportion of slow slip events within slip sequences.
- The observed moment-duration scaling for SSEs depends strongly on the slip rate threshold used to detect events, suggesting instrumental sensitivity influences real-world observations.

CRediT

Conceptualization:	H. S. Bhat
Methodology:	H. S. Bhat, J. Cheng
Software:	J. Cheng, B. Lecampion, P. Dubernet
Investigation:	J. Cheng, H. S. Bhat
Writing - original draft:	J. Cheng, H. S. Bhat
Writing - review & editing:	H. S. Bhat, J. Cheng, B. Lecampion, M. Almakari
Supervision:	H. S. Bhat, B. Lecampion, M. Almakari
Funding acquisition:	H. S. Bhat

Abstract

Traditional models of slow slip events (SSEs) often oversimplify fault geometry, yet imaging studies show that real subduction faults are segmented and complex. We investigate how fault interactions influence slip behavior using 3D quasi-dynamic earthquake sequence simulations of two parallel faults with uniform rate-weakening friction, accelerated with hierarchical matrices. Our results identify four slip regimes—periodic earthquakes, coexisting SSEs and earthquakes, only SSEs, and complex sequences—while a single planar fault under the same conditions produces only earthquakes. We quantify fault interaction using the maximum Coulomb stress induced on a target fault by unit, spatially uniform stress drop on a neighboring fault. Because the source stress drop is normalized, the metric depends only on geometry and is independent of friction and nucleation length, and it can be extended to arbitrary fault configurations. The occurrence of SSEs is confined to an intermediate range of interaction strength. We also reproduce the observed moment-duration scaling and show that it depends on event detection thresholds. These results demonstrate that complex fault geometry can naturally generate both slow and fast earthquakes through evolving traction heterogeneities.

Plain Language Summary

Slow slip events (SSEs) are slow fault movements that release stress gradually, with smaller stress drops and little to no seismic wave radiation, but they still change the stress on the fault and can influence where and when earthquakes occur. Traditional models often assume simple fault geometry, but real faults are complex and can interact with each other. Using 3D simulations of two parallel faults, we show that their basic interactions can generate a wide range of slip behaviors, including periodic earthquakes, slow slip events, and mixed or complex earthquake sequences. A single flat fault under the

same conditions produces only earthquakes, highlighting the importance of fault geometry and interaction. We also find that the transition between slip behaviors depends on how strongly the faults interact each other. These results suggest that the complex geometry of real faults can naturally produce both slow and fast earthquakes observed in subduction zones.

1 Introduction

It has long been recognized that earthquake-related slip accounts for only a fraction of the overall slip budgets within plate tectonics. As continuous geodetic networks have improved, researchers have discovered slow slip events (SSEs) in various tectonic environments, for example in subduction zone: Cascadia subduction zone *(Hirose et al. 1999; Dragert et al. 2001),* in continental strike-slip fault systems e.g., Haiyuan fault *(Jolivet et al. 2013),* San Andreas fault *(Rousset et al. 2019).* These events involve episodic, slow shear motion along faults (a few orders of magnitude faster than plate motion velocity) with no or minimal seismic activity. These events can range from small to large magnitudes, sometimes comparable to earthquakes of the same magnitude. Although SSEs generate little seismic radiation, large-magnitude events can still cause significant stress perturbations and accumulated slip on the fault, affecting its behavior. They are closely linked spatially and temporally with low-frequency earthquakes (LFEs), very low-frequency earthquakes (VLFEs), and tremors, exhibiting a lower frequency of seismic radiation compared to regular earthquakes of same magnitudes. Therefore, seismological instruments can indirectly detect slow slip events by tracking the migration of tremors *(Ito et al. 2007; Shelly et al. 2007; Michel et al. 2018),* repeating earthquakes *(Kato et al. 2012; Uchida 2019),* or LFEs *(Bouchon et al. 2011; Frank & Brodsky 2019),* which improve detection capabilities for slow slip events.

Slow slip events are ubiquitous in subduction zones and exhibit a diverse range of spatiotemporal complexities. Sometimes, they can be observed in shallow depths or below the seismogenic zone. In Nankai Trough, short-term SSEs are discovered with a duration spanning from days to weeks and 3-6 months recurrence time *(Obara et al. 2004; Hirose & Obara 2006)* and long-term SSEs are observed in deep areas with around a 1-year duration and 6-year recurrence time *(Ozawa et al. 2001).* Shallow VLFEs and tremor, megathrust earthquake, long-term SSEs, and short-term SSEs are observed from trough to the deep *(Obara & Kato 2016).* This pattern of depth-dependent SSEs is also seen in the Mexican subduction zone *(El Yousfi et al. 2023).* In Hikurangi, shallow SSEs are accompanied by microearthquakes, and deep SSEs are long-term with a duration of 2-3 months and a recurrence interval of 2 years with no tremors *(Wallace & Eberhart-Phillips 2013).*

Slow slip events (SSEs) have a complex relationship with earthquakes in space and time. In the San Andreas fault, slow and fast rupture can coexist on the same section of the fault *(Shelly 2009; Veedu & Barbot 2016).* Tremor signals were observed 18 months prior to the 2004 Mw 6.0 Parkfield earthquake. There are also examples of SSEs that can occur before earthquakes *(Bürgmann 2018; Martínez-Garzón & Poli 2024).* The 1999 Mw7.6 Izmit earthquake was preceded by a 44-minute slow slip *(Bouchon et al. 2011).* A slow slip event in Guerrero triggered the 2014 Mw 7.3 Papanoa earthquake *(Radiguet et al. 2016).* In the Cascadia subduction zone, GPS observations suggest that the merging of slow slip event fronts, potentially leading to a major earthquake, maybe a possible mechanism for earthquake occurrence *(Bletery & Nocquet 2020).*

Earthquakes can also trigger SSEs. The 2016 Mw7.8 Kaikoura earthquake triggered a slow slip on the southern Hikurangi subduction zone *(Wallace et al. 2018).* The 2017 Chiapas earthquake in Mexico triggered a slow slip event on the southern San Andreas Fault, located 3000 km away from the earthquake's epicenter *(Tymofyeyeva et al. 2019).* SSEs can also occur periodically without earthquakes, like in Cascadia *(Rogers & Dragert 2003)* and Hikurangi subduction zone *(Wallace et al. 2016).* The relationship between earthquakes and SSEs is still unclear and needs more studies and investigation.

Those slow phenomena significantly influence fault behavior by altering the stress field and having intricate relationships with earthquakes *(Avouac 2015; Bürgmann 2018; Obara & Kato 2016).* Understanding slow slip events is crucial for gaining insights into earthquake mechanisms. There are several explanations for the mechanism of SSEs. SSEs can emerge from the transition of rate and state friction stability from velocity-weakening to velocity-strengthening *(Liu & Rice 2005; Rubin 2008).* Heterogeneous frictional properties,

such as varying the proportions of velocity-weakening and velocity-strengthening patches, can produce stable, slow, or dynamic slip events along the fault *(Skarbek et al. 2012; Luo & Ampuero 2017; Nie & Barbot 2021).* Moreover, fault width plays a role in limiting rupture nucleation and stabilizing the faults *(Liu & Rice 2007).* Mechanisms like dilatant strengthening *(Segall et al. 2010; Liu & Rubin 2010)* or frictional restrengthening at high slip speeds *(Kato 2003; Shibazaki & Shimamoto 2007; Im & Avouac 2021)* can modulate fault stabilization and instigate slow slip events. Additionally, thermal instabilities resulting from shear heating and temperature fluctuations can trigger SSEs *(Wang & Barbot 2020).* Furthermore, the brittle-ductile (frictional and viscous deformation) transition *(Nakata et al. 2011; Ando et al. 2023),* viscoelastic materials *(Weng 2025)* and the presence of fluids *(Bernaudin & Gueydan 2018; Cruz-Atienza et al. 2018; Bhattacharya & Viesca 2019; Gao & Wang 2017)* are factors that also contribute to the occurrence of slow slip events.

For a long time, the geometry of subduction interfaces was assumed to be simple, especially when studying slow slip events through other physical mechanisms such as heterogeneous friction or considering fluid as mentioned before. In reality, fault systems possess complex three-dimensional structures. For example, recent imaging of the Ecuadorian subduction zone by *(Chalumeau et al. 2024)* reveals that earthquakes occur across multi-fault segments and subparallel planes, challenging this simplistic view. This complexity emphasizes the need to account for complex fault geometries when studying SSEs. Observations from Hikurangi, including drilling data and seismic reflection images, further highlight the role of material and geometric complexity in promoting slow slip events *(Barnes et al. 2020; Kirkpatrick et al. 2021).* In Cascadia, downdip variability of SSEs suggests a strong geometric influence *(Hall et al. 2018; Mitsui & Hirahara 2006).* Advanced simulations, such as those performed by *Li & Liu (2016)* for Cascadia and *Perez-Silva et al. (2021)* for Guerrero, indicate that non-planar fault geometries are pivotal in understanding SSEs. Fundamental complexities in fault geometry are also considered in SSE modeling, including investigations into precursory slow slip influenced by fault roughness *(Cattania & Segall 2021; Sun & Cattania 2025)* and the emergence of slow slip events from two parallel faults under spatial uniform rate-weakening friction in 2D models *(Romanet et al. 2018).* Recent work by *Almakari et al. (2026)* have highlighted the role of fault zone architecture in producing the complete slip spectrum. Laboratory experiments by *(Kwiatek et al. 2024)* further underscore the complexity, showing both fast and slow ruptures with varying fault slip on rough faults. The effect of stress interaction between multiple faults on slow slip events in 3D models is still unresolved.

In this study, we investigate a step-over configuration of two parallel faults under spatially uniform, rate-weakening frictional conditions to explore the interplay between geometrical and frictional parameters in three dimensions. Three-dimensional simulations of fault slip are computationally intensive, and modeling slow slip events (SSEs) is even more demanding because weakly rate-weakening friction produces large nucleation sizes and requires high temporal resolution. To make such simulations feasible, we use a 3D quasi-dynamic earthquake sequence model based on the boundary element method accelerated with hierarchical matrices *(Cheng et al. 2025; Lecampion et al. 2025)* . Our analysis identifies four distinct slip regimes: (1) only SSEs, (2) SSE-dominant behavior, (3) earthquake-dominant behavior, and (4) only earthquakes. Under identical parameters, a single planar fault produces only earthquakes (Figure. S1), highlighting the critical role of fault geometry in governing slip behavior.

We introduce a fault interaction metric, inspired by fracture mechanics, based on stress perturbations, fault width, length, overlap distance, and spacing, and use it to link geometric complexity with slip behavior through the ratio of SSE to total moment release. Moreover, our simulations reproduce the observed moment-duration scaling across different step-over geometries. The complex spatiotemporal slip patterns arise naturally from evolving traction heterogeneities, or "traction asperities" generated by fault interactions.

2 Method

We used the recently developed numerical approach, FASTDASH which integrates a 3D quasi-dynamic earthquake cycle modelling using boundary element methods accelerated by hierarchical matrices *(Cheng et al.*

2025). This technique significantly optimizes computational efficiency, reducing complexity from $O(N^2)$ to $O(N \log N)$, where N represents the number of discretized fault elements. Such efficiency is crucial for solving complex 3D fault systems effectively. We analyse a fault system with two overlapping faults subjected to a far-field constant stress rate loading. Both faults are governed by laboratory-derived rate and state friction (RSF) law with aging state evolution. Friction is spatial uniform rate weakening. This model includes radiation damping to approximate inertial effect and neglects any wave propagation effect *(Rice 1993).* Both shear and normal traction can vary with slip due to elastic interaction between two faults. With this approach, we can calculate key information on faults including maximum slip rate, moment rate, duration, and the distributions of stress and slip during multiple earthquake cycles.

Linear stability analysis of rate and state friction brings out two important length scales namely the process zone size, L_b, and the nucleation length, L_{nuc}. L_b represents the region where the strength breakdown occurs, and where traction and slip change rapidly. Numerical methods require a sufficient number of grid points within this zone to accurately capture these variations. In this study, we use a grid size of $\Delta s = L_b/3$. On the other hand, L_{nuc} is the critical length necessary for slip instability to occur under idealized conditions. For faults that governed by rate and state friction with ageing law, these parameters are defined as follows: *(Lapusta & Liu 2009; Rubin & Ampuero 2005; Viesca 2016),*

$$L_b = \frac{\mu D_c}{b\sigma_n} \tag{1}$$

$$L_{\text{nuc}} = \begin{cases} 2.7548\, L_b, & 0 \le \dfrac{a}{b} \le 0.3781, \\ \dfrac{2L_b}{\pi\,(1-a/b)^2}, & \dfrac{a}{b} \to 1\,. \end{cases} \tag{2}$$

where μ is shear modulus, D_c is the rate and state characteristic slip distance, a, b are the rate and state friction parameters to represent direct effect and evolution effect. For rate weakening friction, $0 < a/b < 1$. σ_n is the normal traction.

We investigate the influence of geometric and frictional parameters on fault behavior in a three-dimensional compressional step-over configuration. The geometry is characterized by the fault width W, fault length L_f, overlap distance L, and separation distance D between the two faults (Figure 1a). All length scales are normalized by the nucleation length L_{nuc}, which depends on the frictional parameter ratio a/b. The fault aspect ratio is fixed at $L_f/W = 3$. We vary the normalized width W/L_{nuc} from 1.5 to 8 (corresponding to $L_f/L_{\text{nuc}} = 4.5$–24), the overlap fraction L/L_f from 0 to 1, and the normalized separation D/L_{nuc} from 0.1 to 5. Simulations are performed for $a/b \in \{0.4, 0.6, 0.8\}$.

We perform 65 simulations with different geometry and friction setting for our analysis. Table 1 in Supporting Information lists the model parameters that are common to all simulations.

In each simulation, an initial localized slip-rate perturbation is applied to nucleate the first earthquake, after which all subsequent events are included in the analysis. The simulations are run for sufficiently long durations to eliminate the influence of the initial condition. For consistent comparison across different frictional parameters, the total simulation time is chosen to correspond to the duration required for ten earthquakes to occur on a planar fault with the same frictional properties.

3 Results

For a single fault that is longer than L_{nuc} under spatially uniform rate-weakening friction ($a/b < 1$), only periodic earthquake will occur *(Liu & Rice 2005; Rubin 2008).* By considering a fault system with two parallel faults, spatio-temporal complex slip events emerge due to the time dependent evolution of traction heterogeneities produced by fault interaction (Figure 1).

Table 1: Model and geometric parameters used in the simulations.

Friction and material parameters			
Parameter	Description	Value	
a	RSF direct effect parameter	0.008	
b	RSF evolution effect parameter	0.01	
D_c	Characteristic slip distance	0.001 m	
V_{ref}	Reference slip rate	10^{-6} m/s	
f_0	Reference friction coefficient	0.6	
μ	Shear modulus	30 GPa	
ρ	Density	2670 kg m^{-3}	
C_s	Shear wave velocity	3464 m/s	
ν	Poisson's ratio	0.25	
V_0	Initial slip rate	10^{-9} m/s	
$\dot{\tau}_s$	Shear loading rate	0.05 Pa/s	
Geometric parameters			
Parameter	Description	Model 1	Model 2
L_{nuc}	Nucleation length	477.46 m	477.46 m
D	Fault separation	47.746 m	47.746 m
W	Fault width	954.92 m	1909.80 m
L_f	Fault length	2864.80 m	5729.50 m
L	Overlap distance	1432.40 m	2864.80 m

We classify earthquakes and slow slip events based on their slip rates. An event is considered an earthquake if its maximum slip rate is greater than 10^{-3} m/s. Slip rate of slow slip events is typically 1 to 2 order higher than plate rate. In our study, if the maximum slip rate falls between 10^{-8} m/s and 10^{-3} m/s, it is identified as a slow slip event. Various slow slip events, as well as earthquakes having partial or full ruptures are identified in the synthetic catalog (Figure 1(d)). With various combinations of geometry and friction parameters, we identify four regimes: only slow slip events, SSE-dominant, earthquake-dominant and only earthquakes (Figure S2 and S3). We present the spatial-temporal complex events generated from our simulations and reproduce the moment-duration scaling law in this section.

3.1 Spatial-temporally complex events

We show that the step-over configuration generates a wide range of spatiotemporally complex events, with both event durations and inter-event times varying substantiall between events. To illustrate the transition between SSE-dominant and earthquake-dominant regimes, we discuss two examples: Model 1 and Model 2. The parameters are detailed in Table 1. By increasing the fault width, W from $2L_{nuc}$ to $4L_{nuc}$, we observe a shift from SSE-dominant to earthquake-dominant behavior. In Model 1, slow slip events dominate the slip catalog, with only three earthquakes on each fault during the time span in which ten earthquakes occur on a single fault. In Model 2, we observe periodic earthquakes with two slow events occurring during the interseismic period. We selected four events from these two simulations to display the slip distribution on two fault planes (Fig. 1d), illustrating both SSEs and earthquakes occurring on the same faults with partial and full ruptures. Especially in Model 2, events E, F, G, and H form a chain of events, repeating on both faults.

In the SSE-dominant regime, we observe full-rupture SSEs (Event A). In contrast, in the earthquake-dominant regime, SSEs are limited in extent (Events F and G), resulting in less moment released by SSEs in total catalog. We also observe coalescence of two slow slip fronts and merge to a more energetic event (Figure S4).

By increasing fault width, the increased interaction between the faults results in larger stress perturbations, which in turn lead to more frequent earthquakes dominating the sequence of slip events. However, the inter-

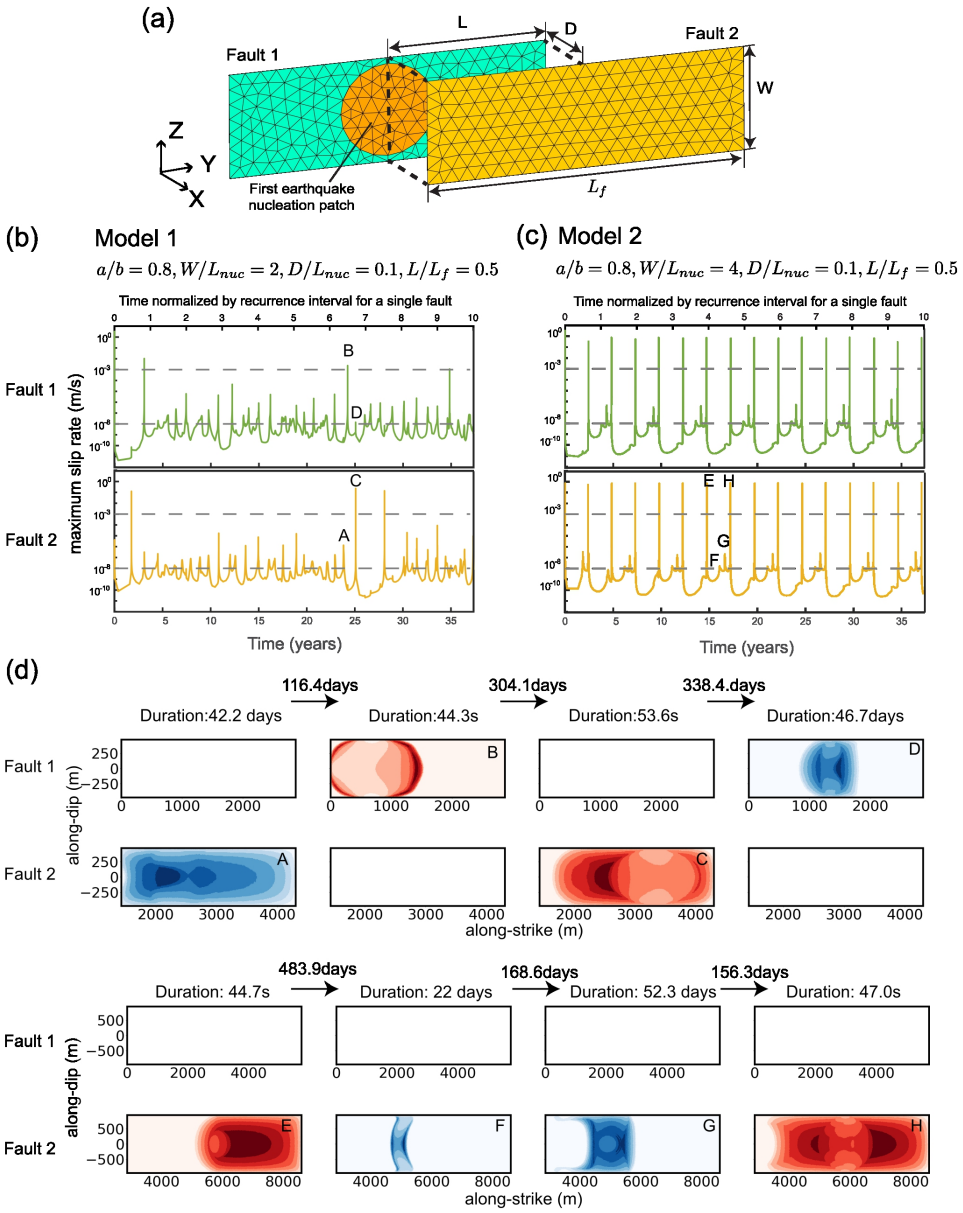

Figure 1: (a) Step-over fault configuration. The mesh is shown exaggerated for visualization purposes; all simulations use a grid spacing of $L_b/3$ (b-c) Example of SSE-dominant regime and earthquake-dominant regime. Time evolution of the maximum slip rate. The bottom x-axis shows real time, while the top x-axis shows time normalized by the recurrence interval of a single fault with the same frictional properties. Green curve is on fault 1 and yellow curve is on fault 2. Grey dash lines are slip rate threshold for earthquakes and slow slip events (d) Spatial distribution of nomalized slip for slip sequences with selected events A, B, C, D in simulation showing in (b) and E, F, G, H in simulation showing in (c). Blue represents slow slip events and red represents earthquakes. Event A is slow slip event with full rupture. Event D, F and G are slow slip events with partial rupture. Event B and E are earthquakes with partial rupture. Event C and H are earthquakes with full rupture. Red and blue color shows normalized slip for earthquakes and slow slip events.

action strength is also controlled by other geometrical parameters L, D and L_f. We discuss the effect of other geometrical parameters in Section 4.1.

3.2 Moment-duration scaling law

We perform seismic cycle simulations with various geometric and friction parameters, generating an extensive dataset in which slip events span several orders of magnitude in rupture area, slip, moment, and duration.

We analyzed slip sequences from each simulation over an equivalent time period (the duration required for a single fault to have 10 earthquakes). We generated moment-duration scaling plots for both slow slip events (SSEs) and earthquakes (EQs), revealing different scaling behaviors: earthquakes exhibit cubic scaling, whereas SSEs follow linear scaling.

Our results show that the moment–duration scaling of slow slip events depends strongly on how the events are defined. Lower slip-rate thresholds detect more events and include slower portions of slip, which increases the inferred duration and moment and modifies the scaling relation. Using a threshold of $10^{-8}m/s$, we identify 1925 SSEs with a scaling $M \sim T^{1.2}$. Increasing the threshold to $10^{-6}m/s$ reduces the catalog to 640 events and steepens the scaling to $M \sim T^{1.5}$. Because this scaling is fitted over the entire population, the resulting exponent represents an average over multiple slip regimes.

Looking in more detail, large SSEs (moment 10^{12}–$10^{16}N \cdot m$) approach cubic scaling. A possible explanation is that small, slow events are dominated by slip accumulation over a nearly fixed area, leading to near-linear scaling, whereas larger events involve significant rupture growth and therefore approach cubic scaling due to three-dimensional effects. The wide scatter likely reflects event-to-event variability in rupture velocity.

These results highlight the sensitivity of SSE detection and inferred scaling to the chosen slip-rate threshold and emphasize the need for consistent event definitions when comparing SSE dynamics across studies *(Almakari et al. 2026; Costantino et al. 2026).*

For earthquakes, the scaling is insensitive to the detection threshold and consistently follows cubic scaling. The observed scatter may result from variations in rupture velocity between events.

4 Discussion

4.1 A metric of to quantify fault interaction

The coexistence of slow slip events (SSEs) and earthquakes (EQs) is significantly influenced by stress perturbations from neighboring faults. When these interactions are considered in a three-dimensional context, the complexity increases notably. Currently, there is no quantified approach to explain how geometrical complexities—such as overlap distance L, distance between faults D, and fault dimensions W and length L_f—control the coexistence of slow and fast earthquakes. In this study, we introduce a new metric Λ, designed to quantify the maximum stress transferred from the primary fault to an adjacent secondary fault, providing a measure of fault-fault interaction strength. The metric is geometrically derived from fracture mechanics under a unit stress drop in a 2D in-plane framework. We utilize Muskhelisvili-Kolosov complex potentials to obtain full-field solutions for cracks, making Λ a function of all relevant geometrical parameters *(Scheel et al. 2021).* $\Lambda = f(L/L_f, D/L_f)$ as derived in Appendix A. The actual interaction between two cracks is linearly proportional to the average stress drop.

$$\Lambda = \max\left\{-2\Im\left[\Phi'(z)\right] - 2y\Re\left[\Phi''(z)\right] + 2f_s y\Im\left[\Phi''(z)\right]\right\} \tag{3}$$

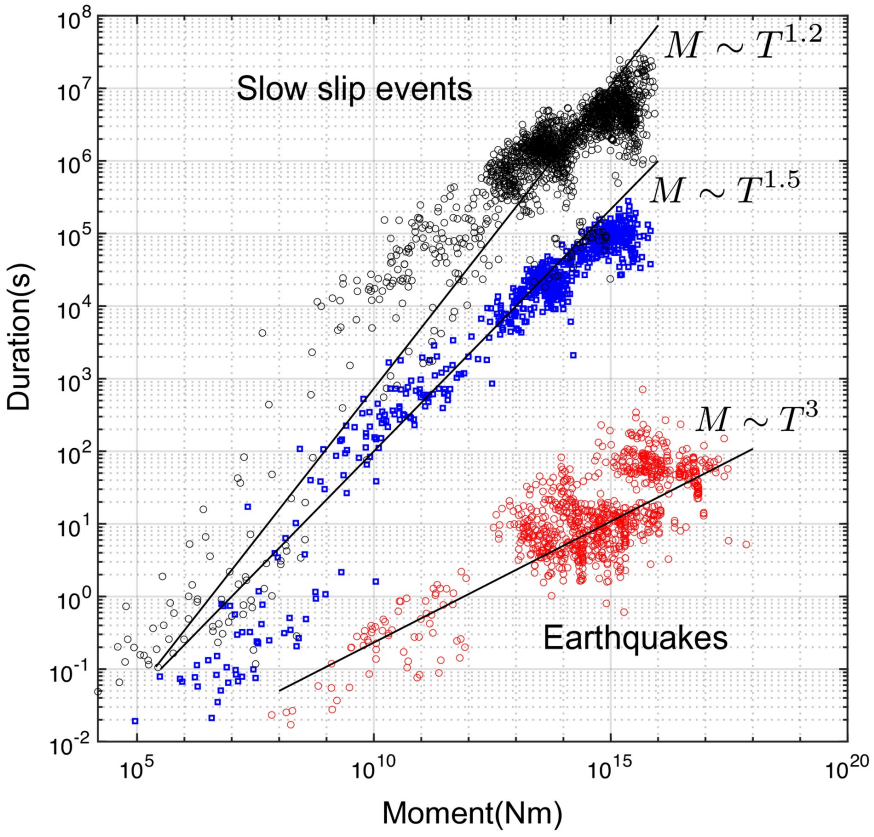

Figure 2: Moment-Duration scaling across all simulations. Red denotes earthquakes exhibiting cubic scaling. Blue and black represent slow slip events identified with slip rate thresholds of $10^{-6}m/s$ and $10^{-8}m/s$, respectively, showing varying but predominantly linear scaling from $M \sim T^{1.5}$ to $M \sim T^{1.2}$

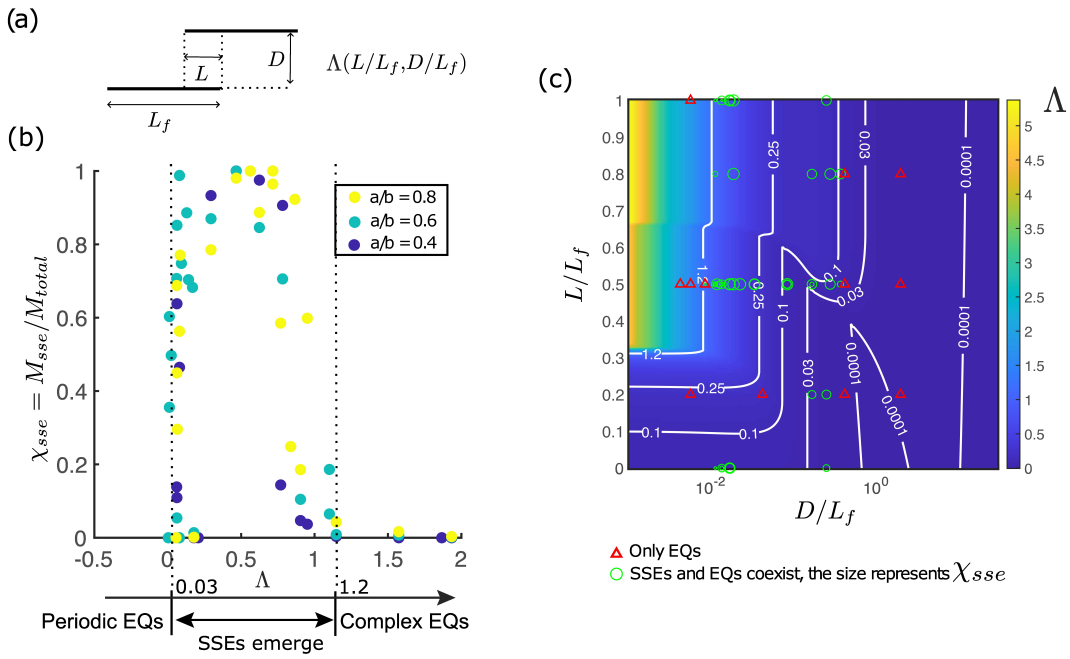

Figure 3: (a) Definition of Λ in relation to the geometric parameters L, D, and L_f (b) The relationship between the fault interaction metric Λ and the SSEs ratio χ_{sse}. Different colored dots represent various friction parameters a/b. The dashed lines indicate that SSEs emerge within a specific range of Λ. Grey area shows the results with SSE-dominant slip catalog. (c) Fault interaction metric Λ as a function of overlap and the distance between two faults, expressed as a fraction of the fault length. The positions of the symbols represent the geometrical configurations in our simulations. Red triangles indicate simulations with only earthquakes, while green circles indicate simulations with coexisting SSEs and EQs, with the size of each green circle corresponding to the SSEs ratio.

where $f_s = 0.6$ is assumed, $z \in [x_1 + iD, x_2 + iD]$ and $x_1 = (2L-1)L_f/2$, $x_2 = x_1 + L_f$. Geometrical parameters are shown in Fig 3(a).

The interaction metric Λ quantifies the stress interaction between faults as a function of their geometrical parameters. Within the tested parameter range, Λ varies from 0 to 2.2 (Fig. 3b). Small Λ values indicate weak or negligible interaction, where the faults are far apart and slip independently. In contrast, large Λ values correspond to strong interaction, occurring when faults are closely spaced or have a large overlap distance, such that their stress fields strongly interact. We further quantify the relative contributions of seismic and aseismic slip using the *SSE ratio* χ_{sse}, defined as the proportion of moment released by slow slip events to the total moment released over ten earthquake cycles for a fault with identical frictional properties. When $\chi_{sse} = 0$, there are only earthquakes; when $\chi_{sse} = 1$, there are only slow slip events. SSEs and EQs coexist when the $0 < \chi_{sse} < 1$. Specifically, SSEs are dominant when $0.5 < \chi_{sse} < 1$, whereas EQs are dominant when $0 < \chi_{sse} < 0.5$.

Our results indicate that geometrical parameters significantly influence the distribution of seismic and aseismic slip (Fig. 3b). When Λ is either too low ($\Lambda < 0.03$) or too high ($\Lambda > 1.2$), faults predominantly host earthquakes. The low Λ values result in periodic earthquakes (Figure S2), while high Λ values lead to complex earthquakes (Figure S3). At the left boundary, $\Lambda \approx 0.03$, the primary controlling factor is the distance between two faults (D). Since Λ is roughly proportional to $1/\sqrt{D}$, the SSE ratio drops rapidly as Λ approaches this boundary. At the right boundary, $\Lambda \approx 1.2$, fault width, W, is the main controlling factor. With Λ being roughly proportional to $\sqrt{W}$, the SSE ratio decreases gradually as it nears this boundary.

However, when Λ falls within an intermediate range ($0.03 < \Lambda < 1.2$), both earthquakes and SSEs can coexist. Within a more specific range ($0.05 < \Lambda < 0.75$), SSEs dominate, shown in Fig 3(b). This is because SSEs are highly sensitive to minor stress perturbations, as noted by *Obara & Kato (2016).* A proper range of interaction is essential to favor slow slip events. If the interaction is too weak, the stress perturbation is insufficient to generate

SSEs. Conversely, if the interaction is too strong, SSEs cannot be sustained and will grow into earthquakes.

We also tested different friction parameters (see in Fig 3b with different colors). For high values of a/b, a slightly wider range of geometrical parameters needs to be considered to identify SSE-dominated regimes. Despite these variations, geometry remains the primary controlling factor. The SSE ratio χ_{sse} can potentially be inferred from these geometrical parameters. This framework provides a mechanical interpretation of how different types of slip events are distributed based on fault geometry.

For a given Λ, various combinations of geometrical parameters can yield the same value. Figure 3(c) illustrates Λ as a function of the overlap and the distance between two faults, expressed as a fraction of the fault length. The value of Λ decreases rapidly with increasing distance between the faults. Λ increases with greater overlap, but when the distance between the two faults is larger, the effect of overlap becomes less significant. Figure 3(c) demonstrates these possible combinations. Most of our simulation results, which feature the coexistence of SSEs and EQs, cover possible combinations where $0.03 < \Lambda < 1.2$. When the geometrical configuration approaches the lower and upper Λ threshold boundaries ($\Lambda = 0.03, \Lambda = 1.2$), the SSE ratio gradually decreases and transitions to only earthquakes. This provides a comprehensive view of how different geometrical configurations influence fault interactions and the coexistence of SSEs and EQs. Additionally, it helps us select appropriate geometrical parameters based on the SSE ratio.

This finding doesn't change with different friction properties, see the circles with different color in Fig. 3(b). This study highlights the critical role of geometrical parameters in understanding and predicting complex slip behavior emerged from fault interaction. Future research should focus on refining these metrics and exploring additional realistic geometrical parameters to further enhance our understanding of the interplay between slow and fast earthquakes in complex fault systems.

Rodriguez Piceda et al. (2025) analyzed normal fault systems by varying along-strike and across-strike spacing separately, focusing on rupture periodicity, synchronicity, and event statistics. In contrast, our study emphasizes the conditions that generate slow slip events. While their analysis treated spacing and overlap distance independently, we introduce a unified fault interaction metric that systematically quantifies how geometric parameters influence both slow and fast slip behaviors. This metric captures the mutual stress interactions between faults, showing that faults "see" each other not merely through geometric distance, but through the stress fields they impose on one another.

4.2 Traction asperities

Notably, our study is based on faults with spatially uniform rate-weakening friction conditions. Previous studies *(Lay et al. 2012; Veedu & Barbot 2016)* used the single planar fault and demonstrated that slow slip events emerge in small asperities with rate-weakening friction and earthquakes occur in large asperities with rate-weakening friction, within the context of friction asperities. Those friction asperities are spatially and temporally stable. Here, we introduce the concept of traction asperities, which naturally arise from multiple fault systems due to stress interactions and previous events. These asperities can also determine the nucleation and arrest of both slow and fast earthquakes.

Figure 4 shows the distribution of the shear-to-normal traction ratio on Fault 2 before and after selected events (E–H) in Model 2 (Figure 1). Owing to stress interactions with neighboring faults and previous ruptures, the traction field exhibits spatial and temporal heterogeneity. For example, the left edge, which overlaps with Fault 1, develops a low traction-ratio patch as a result of fault interaction. Nucleation occurs at regions with a high ratio of shear-to-normal traction asperity (HRA). When the HRA is narrow, nucleation cannot complete within a single asperity, potentially leading to aseismic events (e.g., events F and G). Conversely, regions with a low ratio of shear-to-normal traction (LRA) possess higher strength and act as barriers to arrest events nucleated from the HRA. For example, after nucleation, event E prefers to propagate towards the right HRA and arrests at

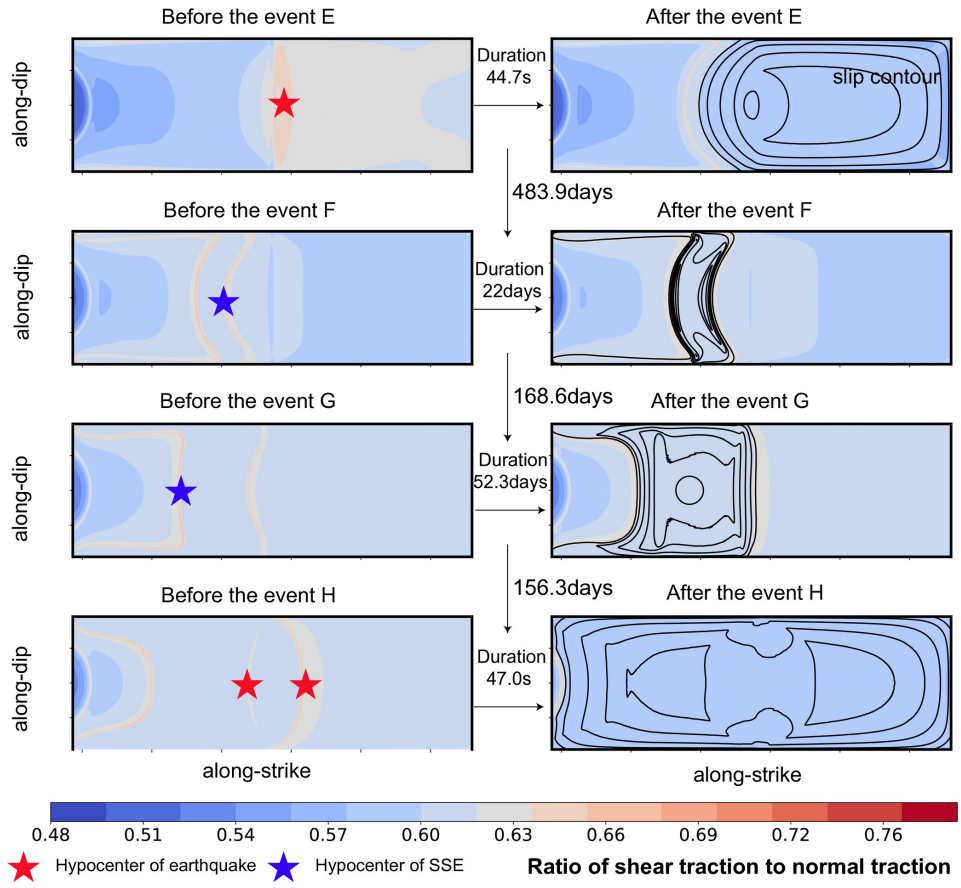

Figure 4: Traction field evolution during four events (E, F, G, and H) on fault 2 in Model 2. The colormap indicates the ratio of shear to normal traction. The first column displays the traction field before the nucleation of each event, with red stars marking earthquake hypocenters and blue stars indicating SSE hypocenters. The second column shows the traction field after each event, with black contour lines representing the slip distribution. The duration of each event and the inter-event times are noted.

the left LRA, resulting in a partial rupture. Same for event F and G, rupture arrests at LRA. The heterogeneity of traction asperities complicates nucleation processes. The coalescence of slip fronts and relatively homogeneous traction fields may lead to full rupture earthquakes, as observed in event H.

4.3 Comparison with single planar fault with heterogeneous friction properties

In this work, we focus on a fault system with two parallel faults and examine the stress interaction between them, leading to a spatio-temporal complex stress field that causes slow slip events and earthquakes with partial and full ruptures. This complexity arises from the dynamic interaction of the faults and their rupture history, rather than from fixed fault parameters. In contrast, models focusing on friction heterogeneity, such as those by *Dublanchet et al. (2013)* and *Kaneko et al. (2010),* suggest that variations in frictional properties can significantly influence seismic behavior. However, frictional heterogeneity is static and once set and does not evolve over time and space, requiring parameter adjustments, such as changes in the sizes, densities, and distances of asperities, to match the observed complexity. Our model demonstrates that simple geometric configurations, like two parallel faults, can naturally produce a wide range of moment-duration laws and complex nucleation patterns, closely mimicking natural seismic and aseismic slip events. Geometric features can be more readily measured using methods like surface rupture tracing and seismic imaging, offering a practical advantage over frictional measurements. Thus, while both geometric complexity and frictional heterogeneity contribute to understanding seismic events, geometric complexity provides a more robust and dynamically evolving framework that can be more readily linked to observations. Future research should integrate these mechanisms to refine

predictive models and enhance our understanding of complex slip events.

5 Conclusion

In this study, we investigate the emergence of complex slow and fast seismic events driven by elastic interactions and heterogeneous stress fields in a three-dimensional fault system composed of two parallel planar faults. Using a 3D quasi-dynamic earthquake cycle model based on the boundary element method accelerated by hierarchical matrices *(Cheng et al. 2025),* we explore how fault geometry and frictional properties control slip dynamics. For a single isolated fault under spatially uniform rate-weakening friction, only regular earthquakes occur when the fault length exceeds the nucleation length. However, when fault interactions are included, stress coupling between neighboring faults generates spatiotemporally complex slip behaviors, including slow slip events (SSEs) and partial or full earthquake ruptures.

We quantify geometric complexity using a fault interaction metric defined as the maximum Coulomb stress change induced on a target fault by unit, spatially uniform stress drop on a neighboring fault. Slip complexity is characterized using the SSE moment release ratio, defined as the fraction of total seismic moment released during slow slip events. SSEs occur only within an intermediate range of interaction strength—too weak or too strong coupling promotes earthquake-dominated behavior—and this pattern remains robust across frictional parameters. Our results also reproduce the moment-duration scaling of SSEs, showing a predominantly linear trend that depends strongly on the slip rate threshold used to identify events. These findings highlight how 3D fault interactions can naturally generate the coexistence of earthquakes and SSEs, bridging the gap between seismic and aseismic slip behaviors.

Acknowledgements

JC, HSB and MA gratefully acknowledge the European Research Council (ERC) for its full support of this work through the PERSISMO grant (No. 865411). The numerical simulations presented in this study were performed on the MADARIAGA cluster, also supported by the ERC PERSISMO grant. BL gratefully acknowledges funding to the EMOD project (Engineering model for hydraulic stimulation) which benefits from a grant (research contract no. SI/502081-01) and an exploration subsidy (contract no. MF-021-GEO-ERK) of the Swiss federal office of energy for the EGS geothermal project in Haute-Sorne, canton of Jura.

Conflict of Interest

The authors declare no conflicts of interest relevant to this study.

Open Research Section

The datasets generated and analyzed during this study, and codes used to analyze, are available at *Cheng et al. (2026).*

Appendix A The definition of fault interaction metric

The Muskhelisvili-Kolosov complex potentials for a shear crack of length $2a$ are given by *(Scheel et al. 2021)*

$$\Phi'(z) = \frac{1}{2i}\left[\frac{z}{(z^2-a^2)^{1/2}} - 1\right] \tag{A.1}$$

$$\Phi''(z) = \frac{1}{2i}\left[\frac{-a^2}{(z^2-a^2)^{3/2}}\right] \tag{A.2}$$

$$\Psi'(z) = -2\Phi'(z) - z\Phi''(z) \tag{A.3}$$

The stress field is then given by $\sigma_{ij}(z) = \sigma^0_{ij} + \Delta\sigma_{ij}(z)$ where

$$\Delta\sigma_{22}(z) = 2y\Im\big[\Phi''(z)\big] \tag{A.4}$$

$$\Delta\sigma_{12}(z) = -2\Im\big[\Phi'(z)\big] - 2y\Re\big[\Phi''(z)\big] \tag{A.5}$$

where $\Re$ and $\Im$ correspond to the real and imaginary parts of their arguments respectively. See figure S5. Length $2a$ is the minimum value of fault length L_f and fault width W. The complex coordinate of fault 2 is denoted as z.

Fault 1 spans from $(-L_f/2, 0)$ to $(L_f/2, 0)$. Fault 2, on the other hand, extends from (x_1, D) to (x_2, D), where $x_1 = (2L-1)\cdot(L_f/2)$, $x_2 = x_1 + L_f$ and L is the overlap.

We define the metric Λ as the maximum of $\Delta\sigma_{12} + f_s\Delta\sigma_{22}$ on fault 2 (figure S6). This metric, which is a function of all geometrical parameters, quantifies the strength of the stress interaction between the two faults.

$$\Lambda = \max\left\{-2\Im\big[\Phi'(z)\big] - 2y\Re\big[\Phi''(z)\big] + 2f_s y\Im\big[\Phi''(z)\big]\right\} \tag{A.6}$$

where $f_s = 0.6$ is assumed.

Supplementary Information for

Quantifying the Role of 3D Fault Geometry Complexities on Slow and Fast Earthquakes

J. Cheng[1,*,¶], H. S. Bhat[1], M. Almakari[1], B. Lecampion[2], P. Dubernet[1]

1. Laboratoire de Géologie, Ecole Normale Superieure, CNRS-UMR 8538, PSL Research University, Paris, France
2. Geo-Energy Lab - Gaznat Chair on Geo-Energy, Swiss Federal Institute of Technology in Lausanne, EPFL-ENAC-IIC-GEL, Station 18, Lausanne CH-1015, Switzerland

∗ Currently at Division of Geological and Planetary Sciences, California Institute of Technology.
¶ Corresponding author: jcheng95@caltech.edu

Introduction

This Supplementary Information provides additional numerical results and simulation parameters supporting the main manuscript. The document is organized as follows:

Supplementary Table:

Table S1 lists the full set of 65 simulations performed, parametrized by a/b, W/L_{nuc}, D/L_{nuc}, and L/L_f.

Supplementary Figures:

Figure S1 shows that a single-fault model produces strictly periodic earthquakes ($a/b = 0.8$, $W/L_{\text{nuc}} = 2$), with a recurrence interval of 3.73 years, serving as the reference baseline for the two-fault stepover simulations.

Figure S2 illustrates the periodic earthquake regime ($\lambda = 0.0183$) for both faults in a stepover configuration with $a/b = 0.8$, $W/L_{\text{nuc}} = 2$, $D/L_{\text{nuc}} = 5$, and $L/L_f = 0.5$, with time normalized by the single-fault recurrence interval.

Figure S3 illustrates the complex earthquake regime ($\lambda = 1.9341$) for $a/b = 0.4$, $W/L_{\text{nuc}} = 8$, $D/L_{\text{nuc}} = 0.1$, and $L/L_f = 0.5$, demonstrating how a wider fault with smaller stepover distance produces irregular recurrence on both fault segments.

Figure S4 shows the slip-rate evolution on the fault plane during the coalescence of two slow-slip events, illustrating the spatial merging process.

Figure S5 presents the shear (σ_{12}) and normal (σ_{22}) stress fields produced by a 2D crack subjected to a unit stress drop, used to validate the stress transfer kernel.

Figure S6 shows the resulting Coulomb stress field $\sigma_{12} + \mu\sigma_{22}$ for a friction coefficient $\mu = 0.6$, highlighting the stress loading and shadowing regions around the fault tips.

ID	a/b	W/L_{nuc}	D/L_{nuc}	L/L_f
1	0.4	1.5	0.1	0.5
2	0.4	2.5	0.1	0.0
3	0.4	2.5	0.1	0.5
4	0.4	2.5	0.1	1.0
5	0.4	2.0	0.1	0.0
6	0.4	2.0	0.1	0.5
7	0.4	2.0	0.1	1.0
8	0.4	2.0	0.2	0.5
9	0.4	2.0	0.5	0.5
10	0.4	2.0	1.0	0.5
11	0.4	3.0	0.1	0.5
12	0.4	4.0	0.1	0.5
13	0.4	4.0	0.5	0.2
14	0.4	4.0	5.0	0.5
15	0.4	6.0	0.1	0.5
16	0.4	6.0	0.1	0.2
17	0.4	6.0	0.1	1.0
18	0.4	8.0	0.1	0.5
19	0.6	1.5	0.1	0.5
20	0.6	1.8	1.5	0.8
21	0.6	1.8	2.0	0.8
22	0.6	2.0	0.1	0.0
23	0.6	2.0	0.1	0.5
24	0.6	2.0	0.1	1.0
25	0.6	2.0	0.2	0.5
26	0.6	2.0	0.5	0.5
27	0.6	2.0	1.5	0.0
28	0.6	2.0	1.5	0.2
29	0.6	2.0	1.5	1.0
30	0.6	2.0	1.0	0.2
31	0.6	2.0	1.0	0.5
32	0.6	2.0	1.0	0.8
33	0.6	3.0	0.1	0.0
34	0.6	3.0	0.1	0.5
35	0.6	3.0	0.1	0.8
36	0.6	3.0	0.1	1.0
37	0.6	4.0	0.1	0.5
38	0.6	4.0	0.5	0.2
39	0.6	4.0	5.0	0.5
40	0.6	4.0	5.0	0.8
41	0.6	4.0	5.0	0.2
42	0.6	6.0	0.1	0.5
43	0.6	8.0	0.1	0.5
44	0.8	1.5	0.1	0.5
45	0.8	1.8	0.1	0.5
46	0.8	1.8	0.1	0.8
47	0.8	1.8	0.1	1.0
48	0.8	1.8	1.5	0.5
49	0.8	1.8	2.0	0.5

continued on next page

Table S1 – *continued from previous page*

ID	a/b	W/L_{nuc}	D/L_{nuc}	L/L_f
50	0.8	2.5	0.1	0.0
51	0.8	2.5	0.1	0.5
52	0.8	2.5	0.1	1.0
53	0.8	2.75	0.1	0.5
54	0.8	2.0	5.0	0.5
55	0.8	2.0	0.07	0.5
56	0.8	2.0	0.1	0.5
57	0.8	2.0	0.2	0.5
58	0.8	2.0	0.5	0.5
59	0.8	2.0	1.0	0.5
60	0.8	3.0	0.1	0.5
61	0.8	4.0	0.1	0.5
62	0.8	4.0	0.5	0.2
63	0.8	4.0	5.0	0.5
64	0.8	6.0	0.1	0.5
65	0.8	8.0	0.1	0.5

Table S1: Simulation parameters.

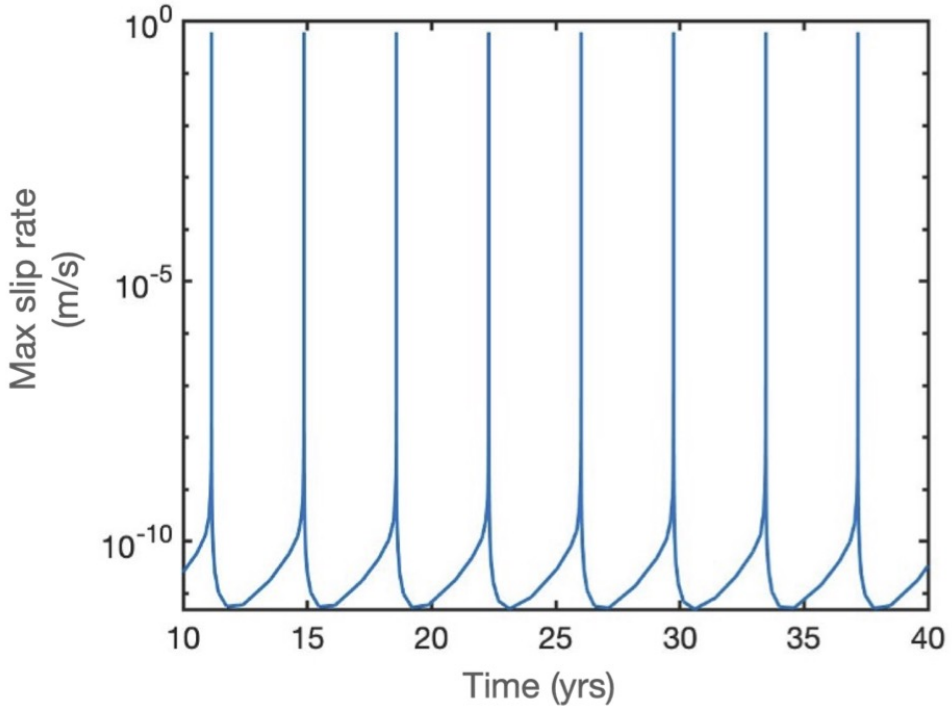

Figure S1: A single-fault model exhibits periodic earthquakes ($a/b = 0.8$, $W/L_{\mathrm{nuc}} = 2$) with a recurrence interval of 3.73 years.

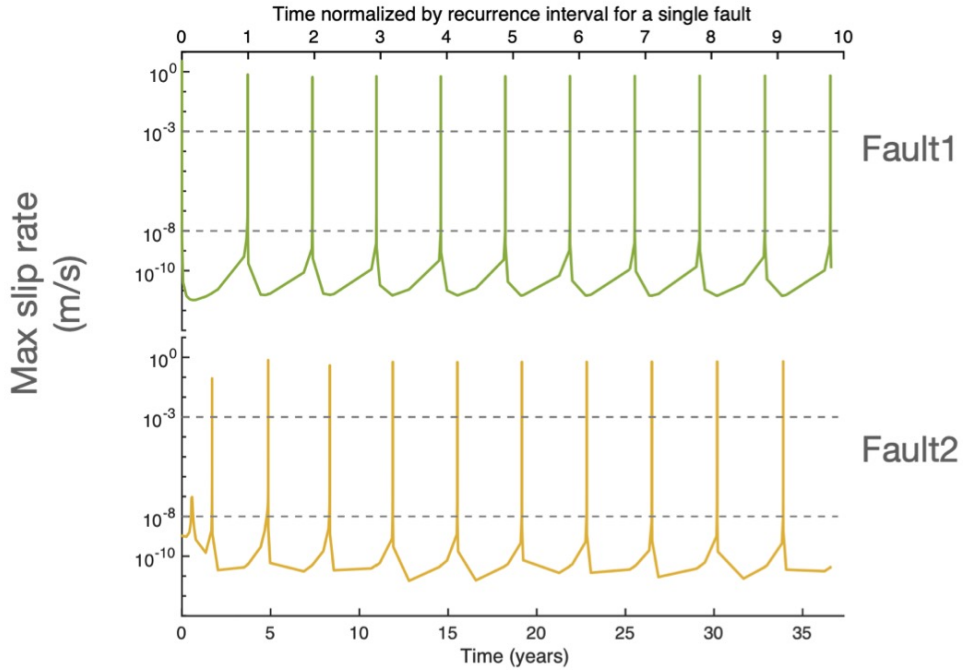

Figure S2: Periodic earthquake regime with $\lambda = 0.0183$ for the simulation with $a/b = 0.8$, $W/L_{\text{nuc}} = 2$, $D/L_{\text{nuc}} = 5$, and $L/L_f = 0.5$.

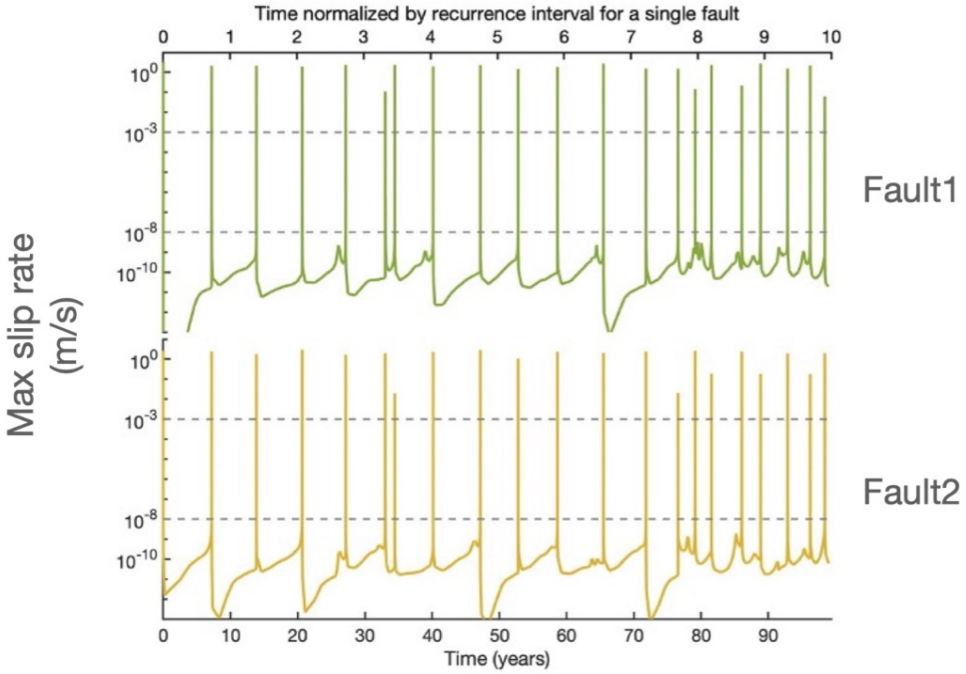

Figure S3: Complex earthquake regime with $\lambda = 1.9341$ for the simulation with $a/b = 0.4$, $W/L_{\text{nuc}} = 8$, $D/L_{\text{nuc}} = 0.1$, and $L/L_f = 0.5$.

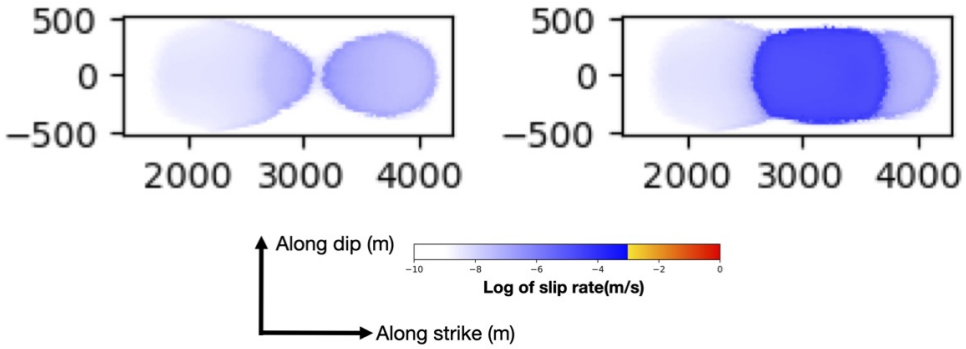

Figure S4: Slip-rate evolution on the fault plane illustrating the coalescence of two slow-slip events.

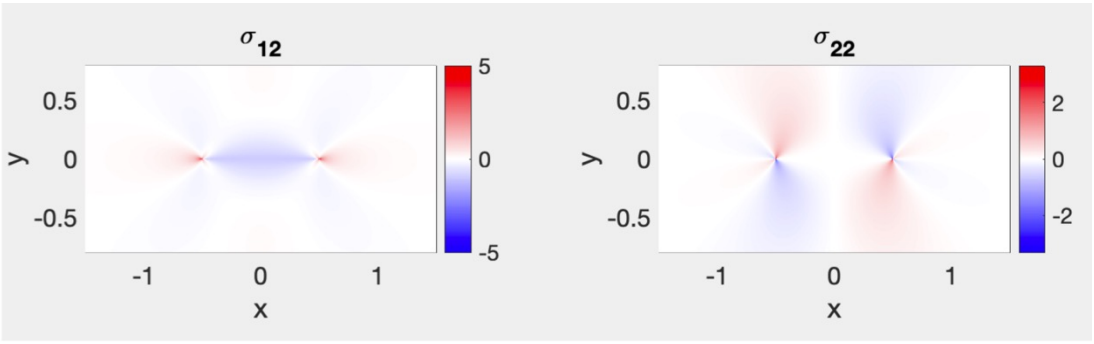

Figure S5: Shear (σ_{12}) and normal (σ_{22}) stress fields produced by a 2D crack subjected to a unit stress drop.

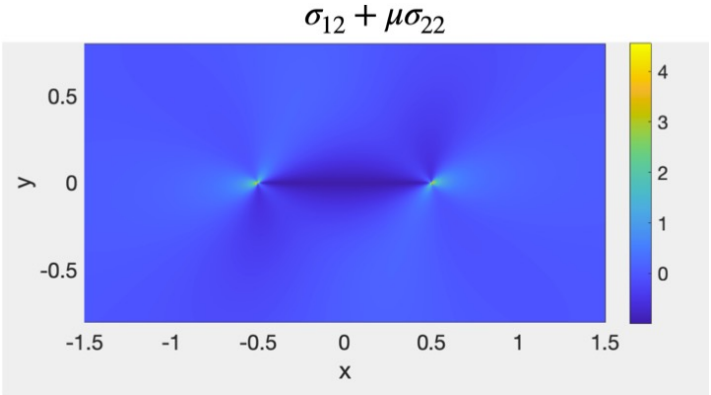

Figure S6: Coulomb stress field $\sigma_{12} + \mu\sigma_{22}$ assuming a friction coefficient of $\mu = 0.6$.

References

Almakari, M., N. Kheirdast, C. D. Villafuerte, M. Y. Thomas, P. Dubernet, J. Cheng, A. Gupta, P. Romanet, S. Chaillat & H. S. Bhat (2026). "Fault volume digital twin to reproduce the full slip spectrum, scaling and statistical laws". In: *under review J. Geophys. Res.* DOI: 10.48550/arXiv.2509.04909. arXiv: 2509.04909.

Ando, R., K. Ujiie, N. Nishiyama & Y. Mori (2023). "Depth-Dependent Slow Earthquakes Controlled by Temperature Dependence of Brittle-Ductile Transitional Rheology". In: *Geophysical Research Letters* 50.5. ISSN: 1944-8007. DOI: 10.1029/2022gl101388.

Avouac, J.-P. (2015). "From geodetic imaging of seismic and aseismic fault slip to dynamic modeling of the seismic cycle". In: *Ann. Rev. Earth Planet. Sci.* 43, pp. 233–271. DOI: 10.1146/annurev-earth-060614-105302.

Barnes, P. M., L. M. Wallace, D. M. Saffer, R. E. Bell, M. B. Underwood, A. Fagereng, F. Meneghini, H. M. Savage, H. S. Rabinowitz, J. K. Morgan, H. Kitajima, S. Kutterolf, Y. Hashimoto, C. H. Engelmann de Oliveira, A. Noda, M. P. Crundwell, C. L. Shepherd, A. D. Woodhouse, R. N. Harris, M. Wang, S. Henrys, D. H. Barker, K. E. Petronotis, S. M. Bourlange, M. B. Clennell, A. E. Cook, B. E. Dugan, J. Elger, P. M. Fulton, D. Gamboa, A. Greve, S. Han, A. Hüpers, M. J. Ikari, Y. Ito, G. Y. Kim, H. Koge, H. Lee, X. Li, M. Luo, P. R. Malie, G. F. Moore, J. J. Mountjoy, D. D. McNamara, M. Paganoni, E. J. Screaton, U. Shankar, S. Shreedharan, E. A. Solomon, X. Wang, H.-Y. Wu, I. A. Pecher & L. J. LeVay (2020). "Slow slip source characterized by lithological and geometric heterogeneity". In: *Science Advances* 6.13. ISSN: 2375-2548. DOI: 10.1126/sciadv.aay3314.

Bernaudin, M. & F. Gueydan (2018). "Episodic Tremor and Slip Explained by Fluid-Enhanced Microfracturing and Sealing". In: *Geophysical Research Letters* 45.8, pp. 3471–3480. ISSN: 1944-8007. DOI: 10.1029/2018gl077586.

Bhattacharya, P. & R. C. Viesca (2019). "Fluid-induced aseismic fault slip outpaces pore-fluid migration". In: *Science* 364.6439, pp. 464–468. ISSN: 1095-9203. DOI: 10.1126/science.aaw7354.

Bletery, Q. & J.-M. Nocquet (2020). "Slip bursts during coalescence of slow slip events in Cascadia". In: *Nature Communications* 11.1. ISSN: 2041-1723. DOI: 10.1038/s41467-020-15494-4.

Bouchon, M, H Karabulut, M Aktar, S Ozalaybey, J Schmittbuhl & M. P. Bouin (2011). "Extended Nucleation of the 1999 Mw 7.6 Izmit Earthquake". In: *Science* 331.6019, pp. 877–880. DOI: 10.1126/science.1197341.

Bürgmann, R. (2018). "The geophysics, geology and mechanics of slow fault slip". In: *Earth Planet. Sc. Lett.* 495, pp. 112–134. DOI: 10.1016/j.epsl.2018.04.062.

Cattania, C. & P. Segall (2021). "Precursory Slow Slip and Foreshocks on Rough Faults". In: *Journal of Geophysical Research: Solid Earth* 126.4. DOI: 10.1029/2020jb020430.

Chalumeau, C., H. Agurto-Detzel, A. Rietbrock, M. Frietsch, O. Oncken, M. Segovia & A. Galve (2024). "Seismological evidence for a multifault network at the subduction interface". In: *Nature* 628.8008, pp. 558–562. ISSN: 1476-4687. DOI: 10.1038/s41586-024-07245-y.

Cheng, J., H. S. Bhat, M. Almakari, B. Lecampion & P. Dubernet (2026). *Quantifying the Role of 3D Fault Geometry Complexities on Slow and Fast Earthquakes*. Zenodo. DOI: 10.5281/zenodo.18168061.

Cheng, J., H. S. Bhat, M. Almakari, B. Lecampion & C. Peruzzo (2025). "FASTDASH: an implementation of 3-D earthquake cycle simulation on complex fault systems using the boundary element method accelerated by H-matrices". In: *Geophysical Journal International* 242.2. ISSN: 1365-246X. DOI: 10.1093/gji/ggaf230. URL: http://dx.doi.org/10.1093/gji/ggaf230.

Costantino, G., M. Radiguet, Z. El Yousfi & A. Socquet (2026). "A Continuum of Slow Slip Events in the Cascadia Subduction Zone Illuminated by High-Resolution Deep-Learning Denoising". In: *Geophys. Res. Lett.* 53.e2025GL117446. DOI: 10.1029/2025GL117446.

Cruz-Atienza, V. M., C. D. Villafuerte & H. S. Bhat (2018). "Rapid tremor migration and pore-pressure waves in subduction zones". In: *Nat. Commun.* 9.1, p. 2900. DOI: 10.1038/s41467-018-05150-3.

Dragert, H., K. Wang & T. S. James (2001). "A silent slip event on the deeper Cascadia subduction interface". In: *Science* 292.5521, pp. 1525–1528.

Dublanchet, P., P. Bernard & P. Favreau (2013). "Interactions and triggering in a 3-D rate-and-state asperity model". In: *J. Geophys. Res.* 118.5, pp. 2225–2245. DOI: 10.1002/jgrb.50187.

El Yousfi, Z., M. Radiguet, B. Rousset, A. Husker, E. Kazachkina & V. Kostoglodov (2023). "Intermittence of transient slow slip in the Mexican subduction zone". In: *Earth and Planetary Science Letters* 620, p. 118340. ISSN: 0012-821X. DOI: 10.1016/j.epsl.2023.118340. URL: http://dx.doi.org/10.1016/j.epsl.2023.118340.

Frank, W. B. & E. E. Brodsky (2019). "Daily measurement of slow slip from low-frequency earthquakes is consistent with ordinary earthquake scaling". In: *Science Advances* 5.10. ISSN: 2375-2548. DOI: 10.1126/sciadv.aaw9386.

Gao, X. & K. Wang (2017). "Rheological separation of the megathrust seismogenic zone and episodic tremor and slip". In: *Nature* 543.7645, pp. 416–419. ISSN: 1476-4687. DOI: 10.1038/nature21389.

Hall, K., H. Houston & D. Schmidt (2018). "Spatial Comparisons of Tremor and Slow Slip as a Constraint on Fault Strength in the Northern Cascadia Subduction Zone". In: *Geochemistry, Geophysics, Geosystems* 19.8, pp. 2706–2718. ISSN: 1525-2027. DOI: 10.1029/2018gc007694.

Hirose, H., K. Hirahara, F. Kimata, N. Fujii & S. Miyazaki (1999). "A slow thrust slip event following the two 1996 Hyuganada earthquakes beneath the Bungo Channel, southwest Japan". In: *Geophys. Res. Lett.* 26.21, pp. 3237–3240.

Hirose, H. & K. Obara (2006). "Short-term slow slip and correlated tremor episodes in the Tokai region, central Japan". In: *Geophys. Res. Lett.* 33.17. DOI: 10.1029/2006GL026579.

Im, K. & J.-P. Avouac (2021). "On the role of thermal stress and fluid pressure in triggering seismic and aseismic faulting at the Brawley Geothermal Field, California." In: *Geothermics* 97, p. 102238. ISSN: 0375-6505. DOI: 10.1016/j.geothermics.2021.102238.

Ito, Y., K. Obara, K. Shiomi, S. Sekine & H. Hirose (2007). "Slow earthquakes coincident with episodic tremors and slow slip events". In: *Science* 315.5811, pp. 503–506. DOI: 10.1126/science.1134454.

Jolivet, R., C. Lasserre, M.-P. Doin, G Peltzer, J.-P. Avouac, J. Sun & R Dailu (2013). "Spatio-temporal evolution of aseismic slip along the Haiyuan fault, China: Implications for fault frictional properties". In: *Earth Planet. Sc. Lett.* 377, pp. 23–33. DOI: 10.1016/j.epsl.2013.07.020.

Kaneko, Y., J.-P. Avouac & N. Lapusta (2010). "Towards inferring earthquake patterns from geodetic observations of interseismic coupling". In: *Nature Geoscience* 3.5, pp. 363–369. ISSN: 1752-0908. DOI: 10.1038/ngeo843.

Kato, A., K. Obara, T. Igarashi, H. Tsuruoka, S. Nakagawa & N. Hirata (2012). "Propagation of Slow Slip Leading Up to the 2011 Mw 9.0 Tohoku-Oki Earthquake". In: *Science* 335.6069, pp. 705–708. DOI: 10.1126/science.1215141.

Kato, N (2003). "Repeating slip events at a circular asperity: numerical simulation with a rate- and state-dependent friction law". In: *Bull. Earthq. Res. Inst.* 78, pp. 151–166.

Kirkpatrick, J. D., Å. Fagereng & D. R. Shelly (2021). "Geological constraints on the mechanisms of slow earthquakes". In: *Nature Reviews Earth Environment* 2.4, pp. 285–301. ISSN: 2662-138X. DOI: 10.1038/s43017-021-00148-w.

Kwiatek, G., P. Martínez-Garzón, T. Goebel, M. Bohnhoff, Y. Ben-Zion & G. Dresen (2024). "Intermittent Criticality Multi-Scale Processes Leading to Large Slip Events on Rough Laboratory Faults". In: *Journal of Geophysical Research: Solid Earth* 129.3. ISSN: 2169-9356. DOI: 10.1029/2023jb028411.

Lapusta, N. & Y. Liu (2009). "Three-dimensional boundary integral modeling of spontaneous earthquake sequences and aseismic slip". In: *J. Geophys. Res.* 114.B9. DOI: 10.1029/2008JB005934.

Lay, T., H. Kanamori, C. J. Ammon, K. D. Koper, A. R. Hutko, L. Ye, H. Yue & T. M. Rushing (2012). "Depth-varying rupture properties of subduction zone megathrust faults". In: *Journal of Geophysical Research: Solid Earth* 117.B4. ISSN: 0148-0227. DOI: 10.1029/2011jb009133.

Lecampion, B., F. Fayard, A. Gupta, C. Peruzzo, A. Sáez, N. Richart, D. Nikolskiy & F. Ciardo (2025). "BigWham: a C++ library for vectorial Boundary InteGral equations With HierArchical Matrices (0.2.0)". Version 0.2.0. In: *Zenodo*. DOI: 10.5281/zenodo.14906635.

Li, D. & Y. Liu (2016). "Spatiotemporal evolution of slow slip events in a nonplanar fault model for northern Cascadia subduction zone". In: *J. Geophys. Res.* 121.9, pp. 6828–6845. DOI: 10.1002/2016JB012857.

Liu, Y. & J. R. Rice (2005). "Aseismic slip transients emerge spontaneously in 3D rate and state modeling of subduction earthquake sequences". In: *J. Geophys. Res.* 110, B08307. DOI: 10.1029/2004JB003424.

Liu, Y. & J. R. Rice (2007). "Spontaneous and triggered aseismic deformation transients in a subduction fault model". In: *J. Geophys. Res.* 112, B09404. DOI: 10.1029/2007JB004930.

Liu, Y. & A. M. Rubin (2010). "Role of fault gouge dilatancy on aseismic deformation transients". In: *J. Geophys. Res.* 115.B10. DOI: 10.1029/2010JB007522.

Luo, Y. & J.-P. Ampuero (2017). "Stability of faults with heterogeneous friction properties and effective normal stress". In: *Tectonophysics*. DOI: 10.1016/j.tecto.2017.11.006.

Martínez-Garzón, P. & P. Poli (2024). "Cascade and pre-slip models oversimplify the complexity of earthquake preparation in nature". In: *Communications Earth & Environment* 5.1. ISSN: 2662-4435. DOI: 10.1038/s43247-024-01285-y.

Michel, S., A. Gualandi & J.-P. Avouac (2018). "Interseismic Coupling and Slow Slip Events on the Cascadia Megathrust". In: *Pure and Applied Geophysics* 176.9, pp. 3867–3891. ISSN: 1420-9136. DOI: 10.1007/s00024-018-1991-x.

Mitsui, N. & K. Hirahara (2006). "Slow slip events controlled by the slab dip and its lateral change along a trench". In: *Earth Planet. Sc. Lett.* 245.1, pp. 344–358. DOI: 10.1016/j.epsl.2006.03.001.

Nakata, R., R. Ando, T. Hori & S. Ide (2011). "Generation mechanism of slow earthquakes: Numerical analysis based on a dynamic model with brittle-ductile mixed fault heterogeneity". In: *J. Geophys. Res.* 116, B08308. DOI: 10.1029/2010JB008188.

Nie, S. & S. Barbot (2021). "Seismogenic and tremorgenic slow slip near the stability transition of frictional sliding". In: *Earth and Planetary Science Letters* 569, p. 117037. ISSN: 0012-821X. DOI: 10.1016/j.epsl.2021.117037.

Obara, K., H. Hirose, F. Yamamizu & K. Kasahara (2004). "Episodic slow slip events accompanied by non-volcanic tremors in southwest Japan subduction zone". In: *Geophys. Res. Lett.* 31.23. DOI: 10.1029/2004GL020848.

Obara, K. & A. Kato (2016). "Connecting slow earthquakes to huge earthquakes". In: *Science* 353.6296, pp. 253–257. DOI: 10.1126/science.aaf1512.

Ozawa, S., M. Murakami & T. Tada (2001). "Time-dependent inversion study of the slow thrust event in the Nankai trough subduction zone, southwestern Japan". In: *Journal of Geophysical Research: Solid Earth* 106.B1, pp. 787–802. ISSN: 0148-0227. DOI: 10.1029/2000jb900317.

Perez-Silva, A., D. Li, A. Gabriel & Y. Kaneko (2021). "3D Modeling of Long-Term Slow Slip Events Along the Flat-Slab Segment in the Guerrero Seismic Gap, Mexico". In: *Geophysical Research Letters* 48.13. ISSN: 1944-8007. DOI: 10.1029/2021gl092968.

Radiguet, M., H. Perfettini, N. Cotte, A. Gualandi, B. Valette, V. Kostoglodov, T. Lhomme, A. Walpersdorf, E. Cabral Cano & M. Campillo (2016). "Triggering of the 2014 Mw7.3 Papanoa earthquake by a slow slip event in Guerrero, Mexico". In: *Nature Geoscience* 9, pp. 829–833. DOI: 10.1038/NGEO2817.

Rice, J. R. (1993). "Spatio-temporal complexity of slip on a fault". In: *J. Geophys. Res.* 98.B6, pp. 9885–9907. DOI: 10.1029/93JB00191.

Rodriguez Piceda, C., Z. K. Mildon, M. van den Ende, J. Ampuero & B. J. Andrews (2025). "Normal Fault Interactions in Seismic Cycles and the Impact of Fault Network Geometry". In: *Journal of Geophysical Research: Solid Earth* 130.4. ISSN: 2169-9356. DOI: 10.1029/2024jb030382. URL: http://dx.doi.org/10.1029/2024JB030382.

Rogers, G. & H. Dragert (2003). "Episodic tremor and slip on the Cascadia subduction zone: The chatter of silent slip". In: *Science* 300.5627, pp. 1942–1943.

Romanet, P., H. S. Bhat, R. Jolivet & R. Madariaga (2018). "Fast and slow earthquakes emerge due to fault geometrical complexity". In: *Geophys. Res. Lett.* DOI: 10.1029/2018GL077579.

Rousset, B., R. Bürgmann & M. Campillo (2019). "Slow slip events in the roots of the San Andreas fault". In: *Science Advances* 5.2. ISSN: 2375-2548. DOI: 10.1126/sciadv.aav3274.

Rubin, A. M. (2008). "Episodic slow slip events and rate-and-state friction". In: *J. Geophys. Res.* 113, B11414. DOI: 10.1029/2008JB005642.

Rubin, A. & J.-P. Ampuero (2005). "Earthquake nucleation on (aging) rate and state faults". In: *J. Geophys. Res.* 110, B11312. DOI: 10.1029/2005JB003686.

Scheel, J., D. Wallenta & A. Ricoeur (2021). "A Critical Review on the Complex Potentials in Linear Elastic Fracture Mechanics". In: *J. Elasticity* 147.1-2, pp. 291–308. DOI: 10.1007/s10659-021-09873-1.

Segall, P., A. M. Rubin, A. M. Bradley & J. R. Rice (2010). "Dilatant strengthening as a mechanism for slow slip events". In: *J. Geophys. Res.* 115, B12305. DOI: 10.1029/2010JB007449,.

Shelly, D. R., G. C. Beroza & S. Ide (2007). "Non-volcanic tremor and low-frequency earthquake swarms". In: *Nature* 446.7133, pp. 305–307. ISSN: 0028-0836. DOI: 10.1038/nature05666.

Shelly, D. R. (2009). "Possible deep fault slip preceding the 2004 Parkfield earthquake, inferred from detailed observations of tectonic tremor". In: *Geophysical Research Letters* 36.17. ISSN: 1944-8007. DOI: 10.1029/2009gl039589.

Shibazaki, B. & T. Shimamoto (2007). "Modelling of short-interval silent slip events in deeper subduction interfaces considering the frictional properties at the unstable–stable transition regime". In: *Geophys. J. Int.* 171.1, pp. 191–205. DOI: 10.1111/j.1365-246X.2007.03434.x.

Skarbek, R., A. Rempel & D. Schmidt (2012). "Geologic heterogeneity can produce aseismic slip transients". In: *Geophys. Res. Lett.* 39.21. DOI: 10.1029/2012GL053762.

Sun, Y. & C. Cattania (2025). "Propagation of Slow Slip Events on Rough Faults: Clustering, Back Propagation, and Re-Rupturing". In: *Journal of Geophysical Research: Solid Earth* 130.2. ISSN: 2169-9356. DOI: 10.1029/2024jb029384.

Tymofyeyeva, E., Y. Fialko, J. Jiang, X. Xu, D. Sandwell, R. Bilham, T. K. Rockwell, C. Blanton, F. Burkett, A. Gontz & S. Moafipoor (2019). "Slow Slip Event On the Southern San Andreas Fault Triggered by the 2017 Mw8.2 Chiapas (Mexico) Earthquake". In: *Journal of Geophysical Research: Solid Earth* 124.9, pp. 9956–9975. ISSN: 2169-9356. DOI: 10.1029/2018jb016765.

Uchida, N. (2019). "Detection of repeating earthquakes and their application in characterizing slow fault slip". In: *Progress in Earth and Planetary Science* 6.1. ISSN: 2197-4284. DOI: 10.1186/s40645-019-0284-z.

Veedu, D. M. & S. Barbot (2016). "The Parkfield tremors reveal slow and fast ruptures on the same asperity". In: *Nature* 532.7599, pp. 361–365. DOI: 10.1038/nature17190.

Viesca, R. C. (2016). "Self-similar slip instability on interfaces with rate- and state-dependent friction". In: *Proc. R. Soc. A*. DOI: 10.1098/rspa.2016.0254.

Wallace, L. M. & D. Eberhart-Phillips (2013). "Newly observed, deep slow slip events at the central Hikurangi margin, New Zealand: Implications for downdip variability of slow slip and tremor, and relationship to seismic structure". In: *Geophys. Res. Lett.* 40.20, pp. 5393–5398. DOI: 10.1002/2013GL057682.

Wallace, L. M., S. Hreinsdóttir, S. Ellis, I. Hamling, E. D'Anastasio & P. Denys (2018). "Triggered Slow Slip and Afterslip on the Southern Hikurangi Subduction Zone Following the Kaikōura Earthquake". In: *Geophysical Research Letters* 45.10, pp. 4710–4718. ISSN: 1944-8007. DOI: 10.1002/2018gl077385.

Wallace, L. M., S. C. Webb, Y. Ito, K. Mochizuki, R. Hino, S. Henrys, S. Y. Schwartz & A. F. Sheehan (2016). "Slow slip near the trench at the Hikurangi subduction zone, New Zealand". In: *Science* 352.6286, pp. 701–704.

Wang, L. & S. Barbot (2020). "Excitation of San Andreas tremors by thermal instabilities below the seismogenic zone". In: *Science Advances* 6.36. ISSN: 2375-2548. DOI: 10.1126/sciadv.abb2057.

Weng, H. (2025). "The Dynamics of Fast and Slow Earthquake Ruptures in Viscoelastic Materials". In: *Journal of Geophysical Research: Solid Earth* 130.6. ISSN: 2169-9356. DOI: 10.1029/2024jb030663. URL: http://dx.doi.org/10.1029/2024JB030663.